Toward Non-contact Muscle Activity Estimation using FMCW Radar

Kukhokuhle Tsengwa, Stephen Paine, Fred Nicolls, Yumna Albertus and Amir Patel

***Abstract*— Surface electromyography (sEMG) and ultrasound-based sonomyography (SMG) are established muscle activity monitoring techniques. However, both modalities require contact with the skin and are thus potentially uncomfortable and time-consuming to use. In this paper, we propose a novel non-contact muscle activity monitoring approach that measures the muscle deformation signal using a Frequency Modulated Continuous Wave (FMCW) mmWave radar which we call radiomyography (RMG). The RMG signal is a specific sequence of phase samples in the radar return, obtained through a series of operations: range bin selection, DC offset correction, arctangent demodulation and phase unwrapping. We find that the RMG signal highly correlates with the sEMG signal across time, making RMG a reliable method for monitoring muscle activity. We also establish that our signal contains some characteristic features of the muscle deformation signal that are well known in biomechanics. Our main contribution is the proposal, development, and proof-of-concept usage of a novel non-contact muscle activity monitoring approach. This opens muscle activity monitoring up for use in rehabilitation, high-intensity contact sports analytics, performance arts, remote health monitoring and wildlife healthcare and research. To the best of the authors' knowledge, our approach is the first to measure the characteristic dimensional changes of muscles in vivo and without contact.**

***Index Terms*— Electromyography, FMCW, mmWave, muscle deformation, Radiomyography, sEMG, Sonomyography**

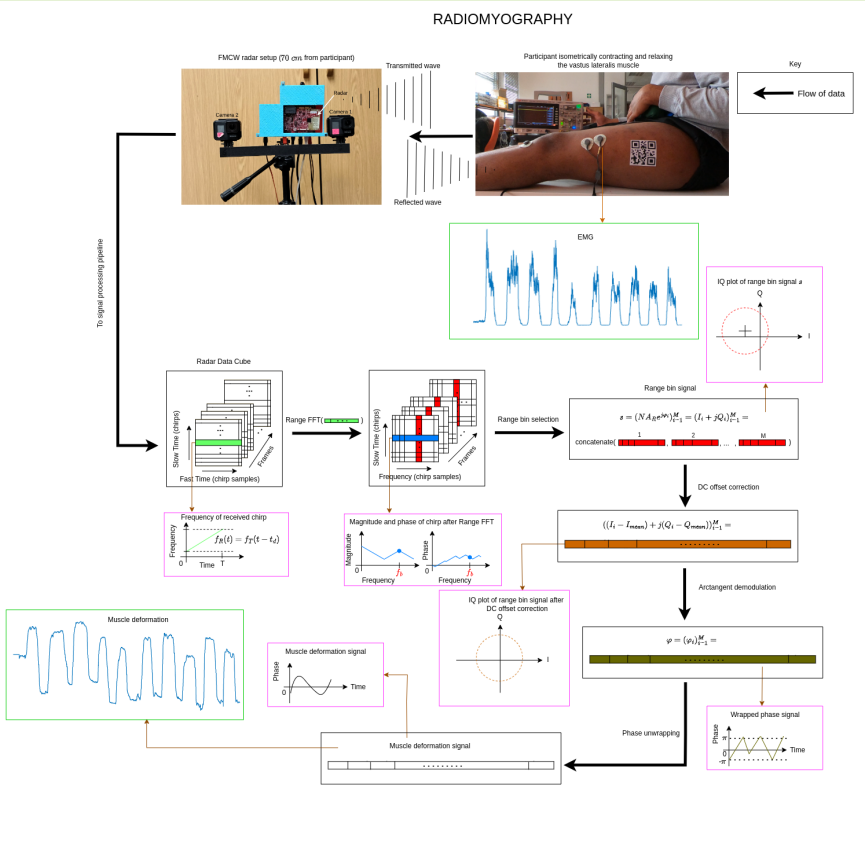

Radiomyography (RMG) monitors the architectural changes on the surface of the skin above a contracting muscle due to the muscle's dimensional changes. The RMG signal is a specific sequence of phase samples in the radar return, obtained through a series of operations: range bin selection, DC offset correction, arctangent demodulation and phase unwrapping.

K. Tsengwa, was with the University of Cape Town, Cape Town, South Africa. He is now with the Oxford Robotics Institute, Department of Engineering Science, University of Oxford, Oxford, UK (e-mail: kukhokuhle@oxfordrobotics.institute).

S. Paine is with the Radar and Remote Sensing Group (RRSG), Department of Electrical Engineering, University of Cape Town, Cape Town, South Africa (e-mail: stephen.paine@uct.ac.za).

F. Nicolls is with the Department of Electrical Engineering, University of Cape Town, Cape Town, South Africa (e-mail: fred.nicolls@uct.ac.za).

Y. Albertus is with the Health, Physical Activity, Lifestyle and Sport (HPALS) Research Centre, Department of Human Biology, University of Cape Town, Cape Town, South Africa (e-mail: yumna.albertus@uct.ac.za).

I. Introduction

MUSCLE activity monitoring is instrumental to clinicians for neurological and orthopaedic rehabilitation [1] [2]. It is also vital as a tool for extracting the signals required for the command of prostheses [1] [3] [4] [5]. Moreover, monitoring muscle activity required for a particular movement aids in the study of that movement, either to better understand the movement or to inform efforts to replicate the movement in robots [6].

Potential difference [7], sound [8] [9] [10], vibration [10] [11] and dimensional changes [3] [11] are the known physical properties whose measurement allows the traditional estimation of muscle activity. Electromyography (EMG) is a muscle activity monitoring approach that measures the potential difference across the cell membranes of muscle cells [7]. Acoustic myography [9] and mechanomyography (MMG) [2] [11] are the names given to the approaches that measure the sound and vibration that occur during muscle activity, respectively. Approaches that measure the dimensional changes of muscles do not yet have an adopted name. Dimensional changes, as measured through ultrasound images, have been referred to as sonomyography (SMG) [12] [13] [14]. However, this name says more about the sensor used than the physical property measured.

EMG is the current state-of-the-art in muscle activity monitoring. Electrical signals, known as action potentials, from the brain travel through motor neurons and cause the muscle fibers innervated by these neurons to be active [7]. Surface EMG (sEMG) thus monitors muscle activity by measuring these electrical signals through surface electrodes placed on the skin over the muscle of interest or through needle electrodes inserted into the muscle [2] [7]. sEMG is thus a contact based approach for the measurement of muscle activity.

The surface electrodes of sEMG require contact with the participant's skin, making sEMG a potentially uncomfortable method for the measurement of muscle activity. Prior to the placement of these surface electrodes, the skin is shaved, rubbed with ethyl alcohol or abrasive conductive paste, washed with water and soap or stripped with adhesive tape to reduce noise and impedance at the electrode-skin interface. Because of tissues between the muscle and electrodes, the sEMG signal may be contaminated by muscle activity from other muscles near the muscle of interest. This is called crosstalk [7]. Moreover, the setup procedure has been termed time-consuming by sEMG experts and is listed as one of the main barriers to the clinical employment of the technique [15].

The low amplitude of the sound produced during muscle activity similarly limits acoustic myography to being a contact based approach. Microphones are often used to measure this signal [10] [11]. Vibration and dimensional changes, however, are properties that can potentially be measured without contact. Indeed, a Laser Doppler Vibrometer (LDV) has been used by Rohrbaugh et al. to measure the vibrations that accompany muscle activity (the MMG signal), in a technique known as Laser Doppler Myography (LDMi) [10] [11] [16]. Dimensional changes as measured through SMG would be technically impractical to measure without contact because of the large difference between the acoustic impedance of air (0.4×10^3 kg·m^{-2}·s^{-1} [17]) and that of human skin (1.99×10^6 kg·m^{-2}·s^{-1} [18]), which would lead to most of the acoustic energy being reflected at the air–skin interface.

It has been shown in previous studies [4] [12] [13] [19] that dimensional or architectural changes in a muscle during its contraction correlate well with the muscle's activity and output force. These informative architectural parameters of muscles include muscle thickness, shape, cross-sectional area, muscle fiber pennation angle and the position of the muscle's surface under the skin. When a muscle contracts, its sarcomeres (the basic contractile units of muscles) necessarily change length [4] [7]. Because the volume of muscles remains constant [20], it follows that muscle activity leads to shape change or deformation of the muscle [4]. It has been demonstrated that this deformation correlates with muscle activity [4] [12] [13] [19]. In most studies, this muscle deformation signal has been measured and the underlying muscle activity monitored by measuring either muscle cross-sectional area, thickness [4] or muscle surface position [12] across a sequence of ultrasound images of the muscle. This approach is known as sonomyography (SMG).

There remains no non-contact muscle activity monitoring approach that measures the characteristic muscle deformation signal seen in the SMG literature. In this paper, we address this gap.

Frequency Modulated Continuous Wave (FMCW) is a specific type of modulation scheme used for active sensors. It is often implemented using radio waves with wavelengths in the millimetre range, a technique known as mmWave FMCW radar. The relatively short wavelengths, compared with traditional radars, allow mmWave radars to be compact and low-cost [21]. Additionally, the high frequencies used (60–64 GHz) allow for wide bandwidths (up to 4 GHz) and thus fine range resolution. The FMCW radar signal is transmitted as frequency modulated sweeps known as chirps. This makes FMCW radars particularly suitable to the monitoring of small motions by analysing the change in phases across the consecutive chirps.

Owing to the properties above, FMCW radar has been

A. Patel is with the Department of Computer Science, University College London, London, UK (e-mail: amir.patel@ucl.ac.uk).

widely and successfully used to measure human vital signs such as heart and breathing rate without contact [22] [23]. With FMCW radar, heart and breathing rates have been measured with a median accuracy of 99% [23]. The non-contact measurement of these signals using FMCW radar is made possible by the movement of the chest in response to the beating of the heart and the inflation and deflation of the lungs. The muscle activity monitoring approach presented in this study was inspired by this prior work.

We propose a non-contact muscle activity monitoring approach that measures the muscle deformation signal using an off-the-shelf mmWave FMCW radar. Our muscle activity monitoring approach measures the small motion at the surface of the skin over the muscle of interest. Our approach measures the same physical attribute measured by sonomyography (SMG) and we have therefore dubbed it radiomyography (RMG). From data collected during trials to evaluate the performance of our system, we observed effects and phenomena that are characteristic of muscles and well known in biomechanics. These are the hysteresis effect between normalised sEMG and normalised muscle deformation signal (see Fig. 10), the exponential relationship between sEMG and muscle deformation (see Fig. 8b) and the higher rate of muscle deformation during the transition from relaxed to contracted muscle state as compared with the transition from a contracted to a relaxed muscle.

The remainder of the paper is organised as follows: Section II introduces the theoretical underpinnings of Frequency Modulated Continuous Wave (FMCW) radar on which our non-contact RMG approach is based. Section III describes the Muscle Activity Estimation Pipeline, detailing the signal processing steps for extracting muscle activity from radar data. Section IV outlines the experimental setup and methodology, providing the context for the validation of RMG against traditional sEMG. The results and their implications are discussed in Section V, showcasing the correlation between RMG and sEMG signals. The paper concludes with Section VI, summarising the main findings and suggesting directions for future research.

II. Frequency Modulated Continuous Wave (FMCW) Radar Theory

The recording of small motions without contact, as we set out to do here, is enabled by the ability of FMCW mmwave radar to encode small motions exhibited by its target as phase information of the complex valued return data. This section details how this is possible, providing context and understanding for subsequent design choices and signal processing.

As the name suggests, the frequency of the transmitted waveform in an FMCW radar is modulated. A sawtooth modulation scheme, known as a chirp, is often used [21]. This means that the frequency of the transmitted waveform, $f_T(t)$, varies linearly with time according to:

$$f_T(t) = \frac{B}{T}t + f_0, \tag{1}$$

where B is the bandwidth of the frequency sweep, T is the time it takes to sweep the bandwidth and f_0 is the starting frequency. This frequency variation across time is why the transmitted signal is called a chirp.

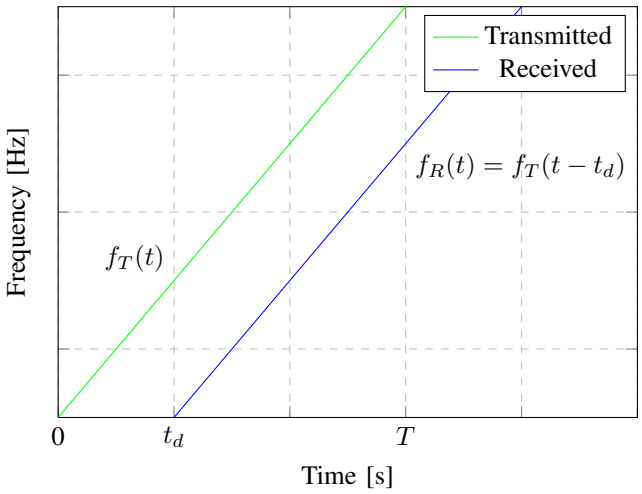

Fig. 1: Frequency of a typical chirp transmitted by an FMCW radar and the frequency of the chirp received by the radar time t_d after the chirp was trasmitted. The transmitted chirp reflected off a target a distance R_0 from the radar.

As seen in [24], a typical chirp transmitted by an FMCW radar can be represented as

$$S_T(t) = A_T e^{j(2\pi f_0 t + \pi K t^2) + \phi_0}, 0 \leq t \leq T, \tag{2}$$

where $K = \frac{B}{T}$ is the slope of the transmitted frequency, ϕ_0 is the initial phase and A_T is the amplitude of the transmitted chirp.

This chirp is transmitted and reflects off a target at a nominal distance of R_0 from the radar. Fig. 1 shows the linearly varying frequency of the transmitted chirp, $f_T(t)$, as well as that of the reflected (or received) chirp, $f_R(t)$. Let $x(t)$ be the component of the target's displacement along the radar's boresight. Then the received chirp, $S_R(t)$, after time t_d becomes

$$S_R(t) = S_T(t - t_d) = A_R e^{j(2\pi f_0 (t - t_d) + \pi K (t - t_d)^2) + \phi_0}, \tag{3}$$

where A_R is the amplitude of the received chirp and the time delay, t_d, is given by

$$t_d = \frac{2(R_0 + x(t))}{c}, \tag{4}$$

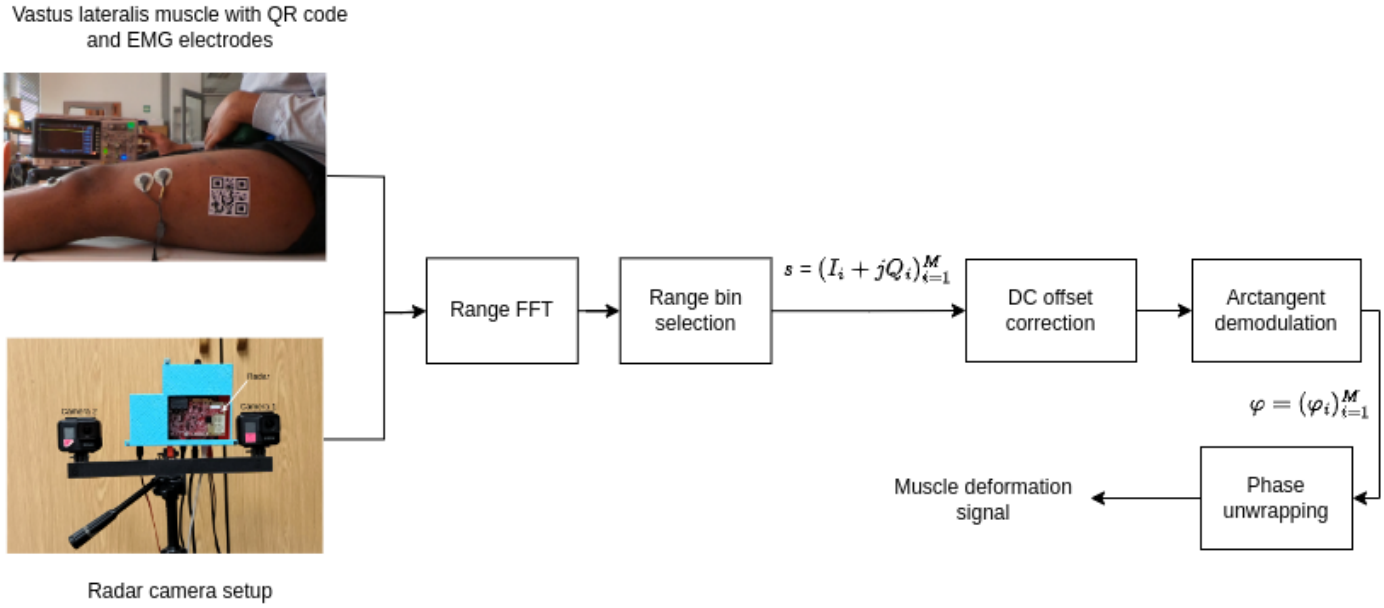

Fig. 2: A flow diagram detailing each stage of the advanced signal processing techniques, from receiving the radar and camera signals to outputting the muscle movement.

where c is the speed of electromagnetic radiation.

The amplitude of the received chirp, A_R, depends on multiple factors such as the peak transmit power of the transmitter, transmit antenna gain, receiver antenna gain, radar cross section (RCS) of the target, the distance between the target and the radar, etc. [21].

In the receiver stage, the signal $S_R(t)$ is amplified by a low noise amplifier (LNA), before being mixed with the original transmit chirp to create the baseband signal known as the beat frequency, before passing through low-pass anti-aliasing filter [21] [24]. A second intermediate frequency (IF) amplification stage is then used before the signal gets digitised. The beat frequency that is digitised, $S_B(t)$, in (5) [24], can be represented as an in-phase component (I) and a quadrature component (Q):

$$S_B(t) = S_T(t) \cdot S_R(t)^* = A_R e^{j(2\pi K t_d t + 2\pi f_0 t_d)}, \quad (5)$$

where $(\cdot)^*$ is the complex conjugate operator.

The term associated with t_d^2 has been ignored since $t_d^2 \ll t_d t$ [24]. Additionally, it has been assumed that during the chirp duration, T, the displacement of the target is negligible and thus the target has no velocity during this time [24]. If this assumption is not made (or is unreasonable), then the frequencies in both $S_R(t)$ and $S_B(t)$ should have a Doppler frequency shift term added to them [21] [24].

Now let us assume that the radar transmits and receives a total of M chirps, each with index $i \in \{1, 2, 3, ..., M\}$. Also suppose that each received chirp has N samples. Then any received chirp can be generally described by

$$\begin{aligned} S_B(iT + t) &= A_R e^{j(\frac{4\pi K R_0}{c} t + \frac{4\pi f_0 R_0}{c} + \frac{4\pi f_c}{c} x(iT))} \\ &= A_R e^{j(2\pi f_b t + \frac{4\pi f_0 R_0}{c} + \frac{4\pi f_c}{c} x(iT))} \\ &= A_R e^{j(2\pi f_b t + \frac{4\pi R_0}{\lambda_0} + \frac{4\pi x(iT)}{\lambda_c})} \\ &= A_R e^{j(2\pi f_b t + \varphi_i)}, \end{aligned} \quad (6)$$

where $f_c = f_0 + \frac{B}{2}$ is the center frequency, λ_c is the center wavelength, $f_b = \frac{2BR_0}{cT}$ is the beat frequency and $\varphi_i = \frac{4\pi R_0}{\lambda_0} + \frac{4\pi x(iT)}{\lambda_c}$.

It is thus clear that the phase of each received chirp, φ_i, encodes within it a sample of the small motion at time iT, $x(iT)$. Just as importantly, we see that the small motion is sampled at frequency $\frac{1}{T}$. Because of the Nyquist–Shannon sampling criterion, this frequency (or equivalently, period) places an upper limit on how fast the target can move while still being unambiguous with this approach. For the value of the chirp duration and the number of transmitters used in our experiments (see Table I), the small motion is sampled at 200 Hz, which is more than required given the rate of muscle contraction and relaxation of the participants in our experiments.

A challenge that faces any approach that monitors a

target's small motion is the presence of larger motions that corrupt the signal of interest. Consider that the target exhibits not only the motion of interest, $x(t)$, but also some other motion, $\rho(t)$, then the recovered phase would be $\varphi_i = \frac{4\pi R_0}{\lambda_0} + \frac{4\pi x(iT)}{\lambda_c} + \frac{4\pi \rho(iT)}{\lambda_c}$. This unwanted motion is called random body motion/movement (RBM) [25]. If RBM is of sufficient magnitude (i.e., exhibits displacements larger than how far the muscle displaces), then the signal of interest can be completely masked.

Due to the corrupting effect of RBM, the current implementation of our system can only monitor muscle activity during isometric contractions. As the muscle lengthens or shortens during eccentric or concentric contractions, the moving body part would introduce RBM. Recommendations for addressing RBM cancellation and thus addressing this limitation are given in the conclusion.

The following section details how the preceding FMCW radar theory informs our system design choices as well as how it is used within our signal processing pipeline to extract the muscle deformation signal from the radar data.

III. Muscle Activity Estimation Pipeline

Through the muscle activity estimation pipeline, we monitor the architectural changes on the surface of the skin above a contracting muscle due to the muscle's dimensional changes. This is achieved by extracting the radar phase signal that encodes the small motion within the radar's field of view as discussed in the previous section. Fig. 2 depicts the different stages in our signal processing pipeline. For a pictorial description of each stage refer to Fig. 3. Each stage is described below.

First, a Discrete Fourier Transform (DFT) was applied on each of the M received chirps at baseband. The frequency axis of this DFT can be interpreted as range and the magnitude of the Fourier coefficients, X_{f_k}, are a measure of how much energy is received from that range. For this reason, this operation is called the Range Fast Fourier Transform (Range FFT).

At the beat frequency, the Range FFT coefficient has magnitude $|X_{f_k}| = NA_R$ whereas at any other frequency the Range FFT coefficient has magnitude $|X_{f_k}| = N^* A_R$, where N is the number of samples per received chirp. We have that $N^* \leq N$ (see the Appendix). Therefore, the magnitude of the Range FFT coefficient at the beat frequency is maximal, i.e., there will not be a Range FFT coefficient with magnitude greater than this one at any other frequency. This is what allows us to determine where the target is, i.e., R_0, accurate to within the range resolution. Often, in practice, $|X_{f_k}| = NA_R$ is not only maximal but is the maximum, which makes finding R_0 easier.

Finding the beat frequency for the target of interest, or equivalently, its nominal distance from the radar, R_0, is what we refer to as the range bin selection stage of our pipeline. Once the beat frequency is known, we extract the Range FFT coefficient at the beat frequency for all received chirps. We call the sequence of all these coefficients the range bin signal, s. From (20), the range bin signal is

$$s = (NA_R e^{j\varphi_i})_{i=1}^{M} = (I_i + jQ_i)_{i=1}^{M}, \tag{7}$$

where I_i and Q_i are the real and imaginary parts of the i^{th} Range FFT coefficient, respectively.

Recall that at the receiver output, the complex-valued baseband signal, $S_B(t)$, in (5) comprises a real and an imaginary part or an in-phase (I) and a quadrature (Q) component, respectively. Ideally, the I and Q components are sinusoids, with a phase offset of $90°$ between each other and with equal amplitudes [21]. In reality, due to imperfections in the receiver's electronics, amplitude and phase imbalances exist between the two channels [21] [26] [27]. Additionally, the range bin signal often contains DC offsets due to coupling effects and environmental interferences [28]. Both of these negatively affect the ability to recover the phase signal and thus must be corrected for.

Through experimenting with different algorithms, we found that the DC offset correction algorithms [21] [29] were very effective at improving phase signal retrieval whereas the IQ imbalance algorithms [21] [27] had no positive effect. The DC offset correction algorithm we specifically implement here subtracts the mean of the range bin signal from the range bin signal. This is represented by the DC offset correction stage in the pipeline.

At the arctangent demodulation stage, the phase signal is obtained from the range bin signal by taking the arctangent of the imaginary part, Q_i, over the real part, I_i, for each sample in the range bin signal [21]. At the output of this stage is the phase signal

$$\varphi = (\varphi_i)_{i=1}^{M}. \tag{8}$$

Because the phase samples, φ_i, in the range bin signal are in the range $[-\pi, \pi]$ (we say the phase is wrapped), after arctangent demodulation it is often necessary to unwrap the phase. This is necessary because if, for example, $x(iT) = \frac{\lambda_c}{4}$, then $\varphi_i = \frac{4\pi R_0}{\lambda_0} + \pi > \pi$ for $R_0 \neq 0$ (see (6)).

Phase unwrapping works by making the assumption that the target does not exceed the maximum permissible velocity, v_{max}, as determined by parameters set on the radar [29] (see Table I).

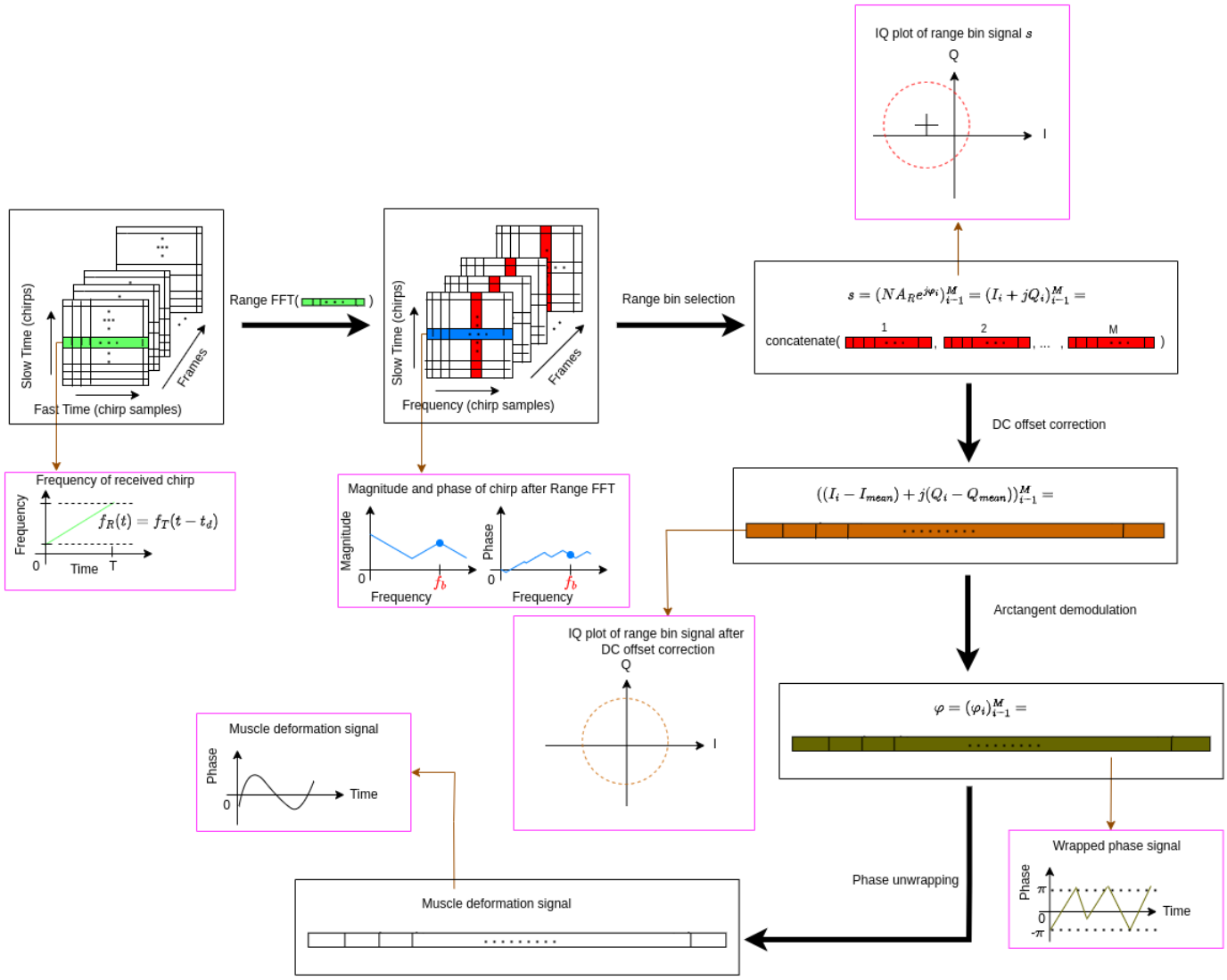

Fig. 3: A detailed pictorial description of the operations within each of the stages of our muscle activity estimation pipeline.

From (6), recall that $\varphi_i = \frac{4\pi R_0}{\lambda_0} + \frac{4\pi x(iT)}{\lambda_c}$. Notice that if, $x((i+1)T) = x(iT) + \frac{\lambda_c}{2}$, then $\varphi_{i+1} = \frac{4\pi R_0}{\lambda_0} + \frac{4\pi x(iT)}{\lambda_c} + 2\pi = \varphi_i$. Even though the small motion has changed by $\frac{\lambda_c}{2}$ over a time duration of $2T$, the phases do not capture this motion. Therefore, we conclude that over a time equal to two chirp times, $2T$, the small motion should change less than $\frac{\lambda_c}{2}$. This argument actually gives us an expression for the maximum velocity, $v_{\max}$, the target can have before it becomes impossible to encode its small motion in the phase. We have

$$v_{\max} = \frac{\frac{\lambda_c}{2}}{2T} = \frac{\lambda_c}{4T} = \frac{\frac{\lambda_c}{4}}{T}. \tag{9}$$

Given the values of the radar parameters used in our experiments (see Table I), we have $v_{\max} = 0.244$ m/s $= 244$ mm/s. For context, the movement of the chest due to normal respiration and heart beat exhibits maximum speeds of 4.08 mm/s and 0.67 mm/s, respectively [30]. In our muscle activity experiments (see Figure 6a), participants contract and relax their muscles at frequencies less than respiration (0.2–0.34 Hz) and heart beat (1–1.34 Hz) frequencies and with amplitudes comparable to chest movements due to respiration 4–12 mm [30].

One interpretation of (9) is that the largest displacement the target can have in a time equal to the chirp time, T, is $\frac{\lambda_c}{4}$. So, given

$$\varphi_i = \frac{4\pi R_0}{\lambda_0} + \frac{4\pi x(iT)}{\lambda_c} \tag{10}$$

and

$$\varphi_{i+1} = \frac{4\pi R_0}{\lambda_0} + \frac{4\pi x((i+1)T)}{\lambda_c}, \tag{11}$$

we have

$$\Delta\varphi = \varphi_{i+1} - \varphi_i = \frac{4\pi\Delta x}{\lambda_c}, \tag{12}$$

where

$$\Delta x = x((i+1)T) - x(iT) \tag{13}$$

Therefore, if the largest value that Δx can attain is $\frac{\lambda_c}{4}$, then the largest value that $\Delta\varphi$ can be is π. Because the target can move towards and away from the radar, we also consider that the displacement Δx cannot be less than $-\frac{\lambda_c}{4}$. This then suggests that the smallest $\Delta\varphi$ can be is $-\pi$. We have

$$-\pi \leq \varphi_{i+1} - \varphi_i \leq \pi. \tag{14}$$

This result leads to the phase unwrapping algorithm proposed in [29] and implemented in the last stage of our pipeline. The algorithm works as follows: iterate over all the wrapped phases. If the difference between two consecutive phases satisfies (14), do nothing. If instead $\varphi_{i+1} - \varphi_i > \pi$, then subtract 2π from φ_{i+1}. Finally, if $\varphi_{i+1} - \varphi_i < -\pi$, then add 2π to φ_{i+1}.

The output of our signal processing pipeline is therefore the unwrapped phase signal, φ, which encodes the small motion exhibited by the target at the nominal distance R_0. In our experimental setup, the radar faced the surface of the skin above the muscle of interest. Assuming that the only motion exhibited by the skin was due to the movement of the muscle underneath it, the phase signal encodes the muscle deformation signal which we use as a measure of muscle activity.

IV. Experiments

We hypothesise that the muscle activity signals recorded by our system will show a high correlation with those captured by the sEMG sensor. Secondly, we hypothesise that our system records the same muscle deformation signal recorded by SMG but without contact. If the first hypothesis is accepted, then this validates the efficacy of our system since sEMG is the gold standard for muscle activity monitoring. The muscle deformation signal, as extracted through SMG, has been shown to be a promising alternative to sEMG with desirable qualities such as participants' preference to use this signal to control icons on a screen [4]. To investigate these hypotheses, we compute the biserial correlation between our muscle deformation signal and the state of the muscle as inferred from sEMG. We also study the mathematical relationship between our signal and sEMG, comparing our results to relationships reported between SMG and sEMG.

TABLE I: Values of the FMCW radar parameters used.

Parameter	Value
Chirp Sweep Time (T)	1670.17 μs
Number of ADC Samples per Chirp (N)	2048
Number of Chirps per Frame	255
Number of Frames	40
Frame Periodicity	1296 ms
Bandwidth (B)	2.45 GHz
Number of Transmitters used	3
Starting Frequency (f_0)	60 GHz

To evaluate the performance of our radar based muscle activity monitoring system, we recruited three participants from which the required data was collected. All participants were aged between 22 and 25 years. During each trial, two sets of time-synchronised data were collected, one from the radar and another from the sEMG sensor. Table I shows the values of the FMCW radar parameters used to record the radar data. Time-division multiplexing multiple-input-multiple-output (TDM-MIMO) was used [31]. The radar and sEMG sensor were triggered using an external hardware trigger.

sEMG data was collected using the wireless TeleMyo 2400T G2 Telemetry System developed by Noraxon. The system consisted of a transmitter which was connected to the sEMG's surface electrodes via leads. The transmitter was then wrapped around the waist of a participant and rested on the lap (see Fig. 4). A receiver then received and sent the sEMG data to a PC via USB. The sEMG data was recorded at a sampling frequency of 1.5 kHz. It was then bandpass filtered with 30 Hz and 200 Hz for the lower and upper cutoff frequencies of the bandpass filter, respectively. Finally, the data was rectified and the envelope obtained through the computation of the RMS with a moving mean with a window size of 100 samples.

Four trials, each roughly 1 minute (57.1 s) long, were conducted on each participant. During a trial, a participant was asked to isometrically contract and relax their vastus lateralis muscle (the strongest and largest quadriceps muscle that runs along the entire length of the lateral side of the thigh) randomly. A pair of sEMG electrodes were placed over the vastus lateralis and one sEMG ground electrode was placed over the patellar tendon (see Fig. 4).

The muscle activity monitoring experimental setup consisted of a Texas Instruments (TI) IWR6843ISK mmWave FMCW radar [32] and the DCA1000EVM data capture board [33]. Both devices were enclosed within a 3D-printed enclosure which was mounted on a 35 cm long rectangular 3D-printed rod. These two devices were connected to the MMWAVE-ICBOOST [34], which received the synchronising signal. On either side of the radar was a GoPro HERO 7 Black camera (see Fig. 5) with frame rate and resolution set to 120 fps and

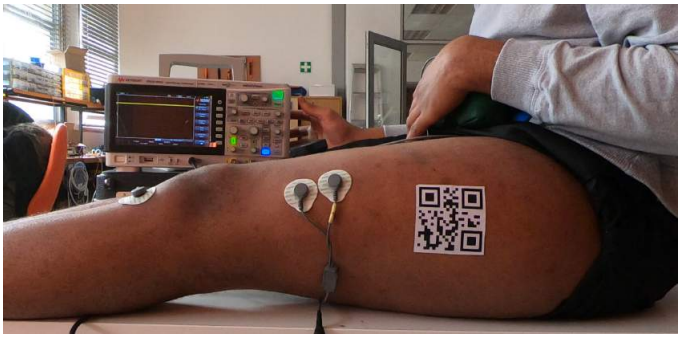

Fig. 4: Each participant sat on top of a table that was placed 70 cm in front of the tripod while wearing shorts to expose the QR code to the cameras.

1920×1080 pixels, respectively. We refer to these as camera 1 and 2 and the data from these cameras was used to corroborate the vastus lateralis' range estimation from the radar. Both cameras were also mounted on the same rod, and the rod was fixed to an adjustable-height tripod. It is important to note that the cameras were completely unnecessary for the operation of the proposed non-contact muscle activity monitoring system.

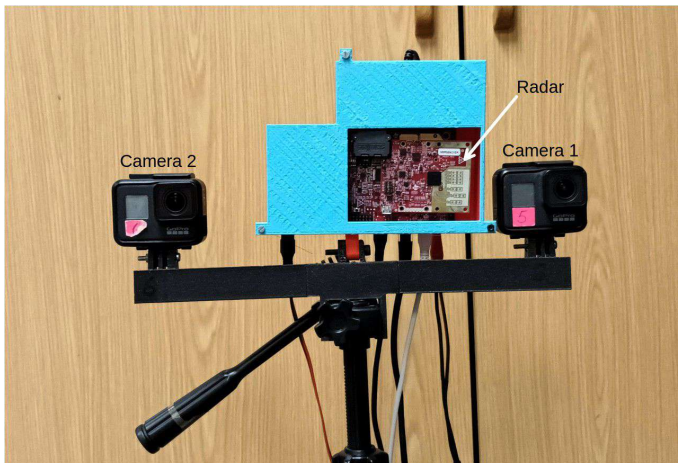

Fig. 5: Our muscle activity monitoring experimental setup consisted of the Texas Instruments (TI) IWR6843ISK mmWave FMCW radar and the DCA1000EVM data capture board. Both devices were enclosed within a 3D-printed enclosure which was then mounted on a 35 cm long rectangular 3D-printed rod. On either side of the radar was a GoPro HERO 7 Black camera.

A QR code was also placed on the skin over the vastus lateralis muscle using paper glue. The skin was shaved with a razor blade for each participant, enabling the QR code to be placed onto the skin surface. The QR code was used together with a calibrated stereo camera pair to estimate how far the vastus lateralis muscle was from the radar using triangulation. This range estimation was used to corroborate the vastus lateralis' range estimation from the radar. Recall that range estimation is equivalent to range bin selection, which was one of the stages in our muscle activity monitoring pipeline. It is to be noted that the radar's range estimation was sufficient and that the QR code was not required at any stage of our pipeline.

Each participant sat on top of a table that was placed 70 cm in front of the tripod while wearing shorts to expose the QR code to the cameras, as presented in Fig. 4. It should be noted, however, that the radar can penetrate through clothing. The tripod's height was adjusted such that the radar's boresight was pointing directly at the participant's vastus lateralis muscle.

Ethical approval for this study was obtained from the University of Cape Town Faculty of Health Sciences Human Research Ethics Committee (HREC REF: 379/2022).

V. Results and Discussion

In section IV we hypothesised that the RMG and sEMG signals are highly correlated. In this section, the biserial correlation coefficient between the root mean square (RMS) value of the RMG signal and the state of the muscle as deduced from the sEMG signal will be used to measure this correlation. To investigate our second hypothesis, which proposes that the RMG signal is analogous to the SMG signal, we will fit an exponential curve to the RMG vs. sEMG data and compare this fit to the existing SMG vs. sEMG relationships reported in the literature.

The results presented here are from a total of 12 trials across the three participants. Four trials were conducted for each participant. Each trial was about 1 minute (57.1 s) long. Fig. 6 illustrates the sEMG and radar phase signals recorded from one such trial, specifically from participant one. We observed that each time the participant contracts the vastus lateralis, the radar phase signal increased. This implies that contraction deforms the vastus lateralis muscle away from the radar. Conversely, when the muscle was relaxed, the radar phase decreased. This suggests that relaxation deformed the muscle towards the radar.

The most noticeable feature of Fig. 6 is the high correlation between the sEMG signal and the deformation signal (as measured by the phase signal). Several other studies [4] [12] [19] have demonstrated that muscle deformation (as measured through ultrasound images) correlates with muscle activity (as measured through sEMG) and/or muscle force.

In order to quantify as well as establish the strength of the correlation depicted in Fig. 6, we calculated the biserial correlation coefficient, r_{pb}, between the RMS value of the radar phase signal and the state of the muscle (relaxed or contracted) as deduced from the ground truth sEMG signal. This coefficient measures the correlation between a continuous variable, in our

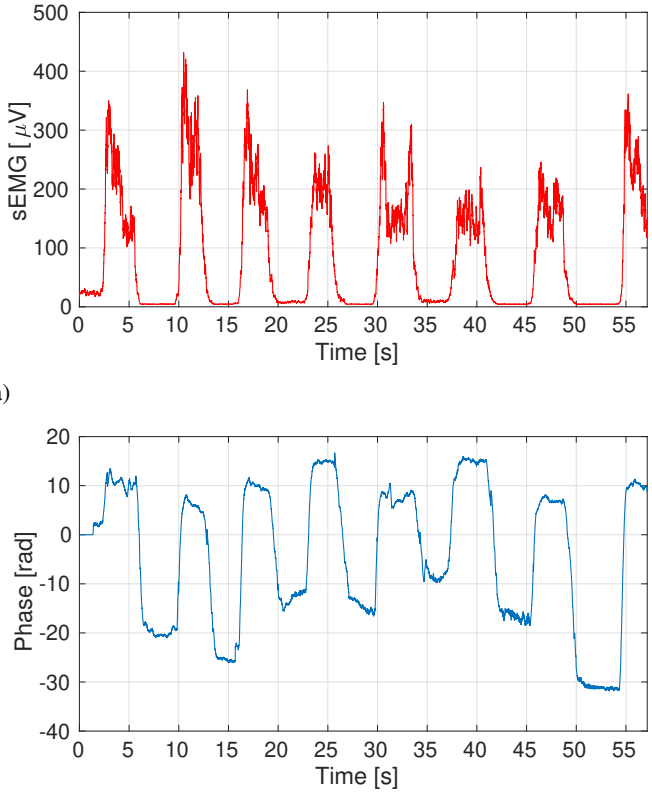

Fig. 6: During each trial, a participant was asked to isometrically contract and relax their vastus lateralis muscle randomly. Two sets of time-synchronised data were then collected. These are (a) sEMG and (b) radar data as presented here. The data in this figure is generally typical across subjects. Observed differences are in the time duration for which each participant activates the muscle as well as the level of activation for each participant (i.e., amplitude of each signal), which both should be expected since participants contracted and relaxed randomly.

case the RMS of the radar phase, and a dichotomous variable, the muscle's state in our case. It is computed as

$$r_{\text{pb}} = \frac{\bar{\varphi}_{1\text{rms}} - \bar{\varphi}_{0\text{rms}}}{\sigma_n} \sqrt{\frac{n_0 n_1}{n^2}}, \tag{15}$$

where $\bar{\varphi}_{1\text{rms}}$ and $\bar{\varphi}_{0\text{rms}}$ are the mean RMS of the radar phase in the contracted state and relaxed muscle state, respectively. Additionally, σ_n is the standard deviation of all the RMS values data, n_1, n_0 and n are the number of radar phase RMS values in the contracted state, relaxed state and the total number of radar phase RMS values in the data, respectively.

The RMS is a commonly used metric in the analysis of muscle activity signals [10] [12]. As can be seen in Fig. 6, the radar phase signal goes below 0 rad when the muscle is in the relaxed state. In order to preserve the directionality of

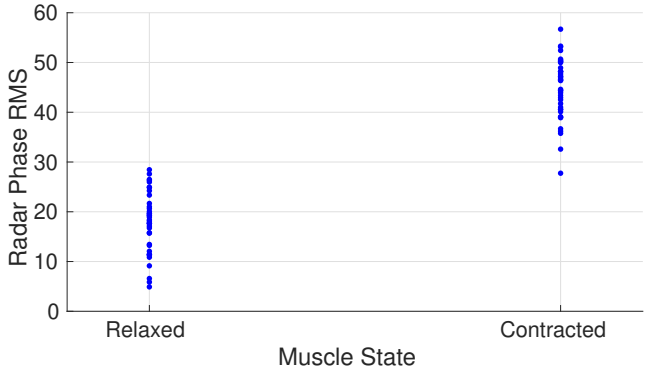

Fig. 7: Showing the RMS value of the radar phase signal against the state of the muscle. The data presented is from all four trials of participant one. The plot depicts the correlation between the RMS value of the radar phase signal and the state of the muscle as deduced from the corresponding sEMG signal.

this signal during the computation of the RMS, the absolute value of the minimum radar phase across all four trials was added to all radar phase signals to bias them above 0 rad.

Using the data from all the four trials of participant one, the biserial correlation coefficient was calculated to be 0.91 or 91%. This is a strong positive correlation suggesting the deformation signal as measured by our system can be reliably used to monitor or classify the muscle's state. We therefore claim that the hypothesis that the SMG signal is highly correlated to sEMG is accepted. Fig. 7 shows the data used to compute the reported correlation coefficient. The data consists of 40 and 38 RMS values corresponding to the contracted and relaxed states, respectively.

An exponential relationship between sEMG and SMG-measured muscle deformation has been observed in the literature [12] [35], and our data corroborates this relationship, providing evidence that RMG is measuring a signal similar to that of SMG. Particularly, this exponential relationship was observed between deformation, as measured through normalised radar phase, and normalised sEMG. The signals are normalised by dividing each sample by the largest sample in the signal. Fig. 8b presents a scatter plot of normalised radar phase against normalised sEMG for the first contraction in Fig. 6. The exponential relationship between the two variables can be seen in this plot.

Also depicted in Fig. 8b is an exponential curve that best fits the data. Following [12] and [35], the best fit line was modelled as

$$\hat{Y} = \hat{A}(1 - e^{-\hat{B}\hat{X}}), \tag{16}$$

where $\hat{Y}$ is the normalised muscle deformation, $\hat{X}$ is the

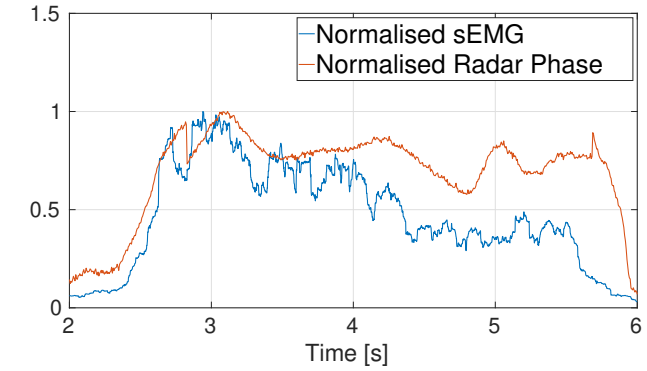

(a)

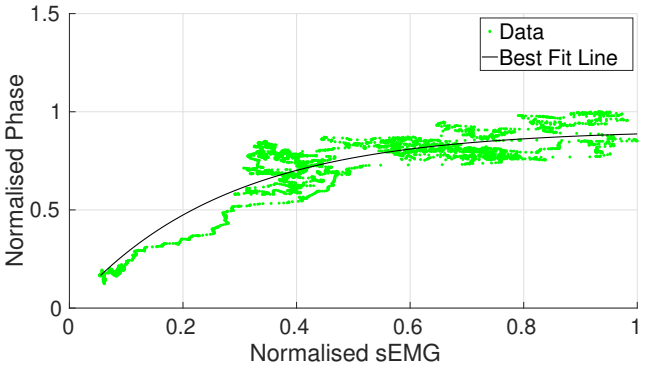

(b)

Fig. 8: Illustrated in (a) is the normalised sEMG and corresponding normalised radar phase from a single contraction-relaxation cycle in Fig. 6. The relationship observed between the two normalised signals is characteristic of muscles and, represented differently, it results in the hysteresis curve in Fig. 10. A scatter plot of the normalised radar phase against normalised sEMG during the contraction phase of (a) is presented in (b). Also included in (b) is the exponential line that best fits the data. The exponential relationship observed here is typical.

normalised sEMG, $\hat{A}$ is the asymptotic value of $\hat{Y}$ and $\hat{B}$ is the exponent coefficient determining the curvature.

To solve for the model coefficients $\hat{A}$ and $\hat{B}$, MATLAB's lsqnonlin() method from the Optimisation Toolbox was used to fit (16) to the data. The problem was posed as a non-linear least-squares curve fitting problem and solved using the Levenberg–Marquardt algorithm [36]. For the data in Fig. 8b, the values of $\hat{A}$ and $\hat{B}$ were found to be 0.91 and 3.68, respectively. The equation of the depicted best fit line is thus $\hat{Y} = 0.91(1 - e^{-3.68\hat{X}})$. The model coefficients were calculated for all 12 experiments. Fig. 9 presents the 12 values of each coefficient across participants and experiments.

The plots shown in Fig. 8a can be considered in two stages, the ON or contraction stage from roughly 2 s to 3 s and the

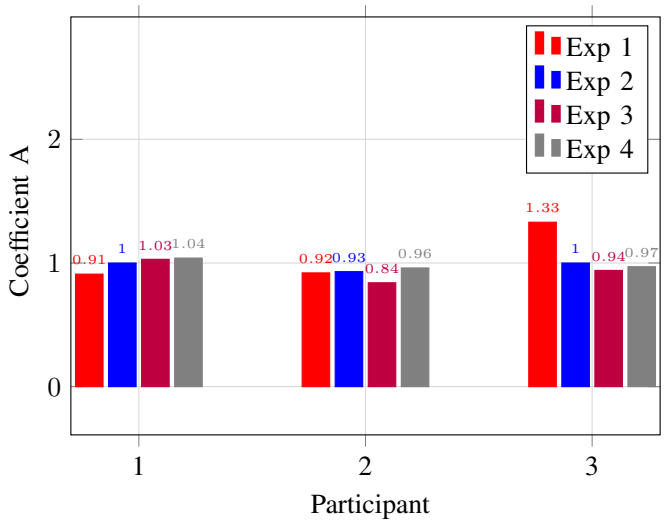

(a)

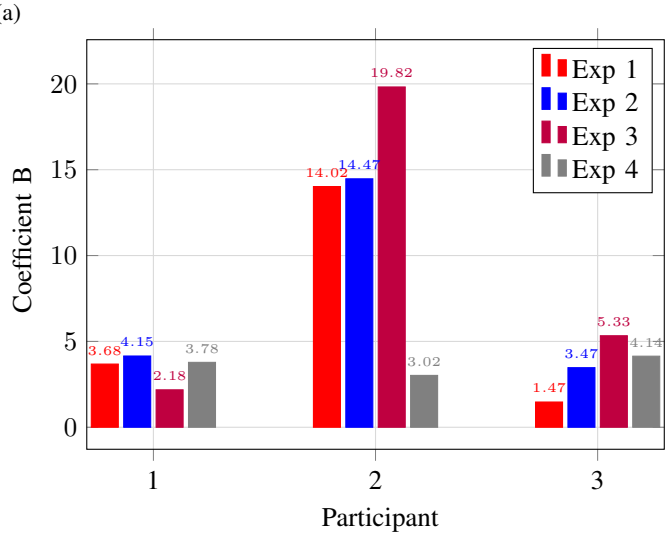

(b)

Fig. 9: The relationship of normalised radar phase to normalised sEMG during the contraction of a muscle has been observed to be exponential, as depicted in Fig. 8b. Equation (16) is often used to model the relationship and we do the same here. In (a) is the value of coefficient A and in (b) is the value of coefficient B for the data collected from all the trials viewed per participant.

OFF or relaxation stage from roughly 5.5 s to 6 s. The ON stage refers to the transitory period from a relaxed muscle state to a contracted state and the OFF stage refers to the transitory period from a contracted to a relaxed muscle state. In practice, the start of the ON stage and the end of the OFF stage were delineated by the time the signal goes above or below a lower threshold value, respectively. The end of the ON stage and the beginning of the OFF stage were delineated by the time the signal goes above or below an upper threshold value,

respectively. For the normalised signals, these can be selected as percentages of the maximum signal value, i.e., values between 0 and 1. What stands out in this figure is that muscle deformation significantly lags behind the decreasing sEMG during relaxation whereas it closely correlates with sEMG during contraction. In this respect, our data also corroborates existing literature [37] [38] about certain mechanical muscle characteristics (e.g., force) depending not only on the level of excitation but also on the prehistory of contraction.

Notice that a given percentage of muscle deformation (normalised radar phase) corresponds to a lower percentage sEMG during the OFF stage than during the ON stage. This phenomenon is easily observable when the normalised sEMG is plotted against the normalised radar phase for only the ON and OFF stages. Fig. 10 depicts such a plot, drawn from the data in Fig. 8a. The resultant curve is called a hysteresis curve and was also observed in [12] and [39]. In [12], the hysteresis was between muscle deformation and sEMG and is exactly as we observed here. In [39] however, it was observed between muscle deformation and force and it was stated that such hysteresis curves are well known in biomechanics. The sEMG amplitude increased during the ON stage and decreased during the OFF stage, and therefore the hysteresis in Fig. 10 (and [12]) has a clockwise direction while that in [39] has an anti-clockwise direction. Existing literature has shown that there is extreme variability in the manifestations of these hysteresis loops and that their directions, in particular, can be different [38] [40]. Based on the observed exponential relationship between the normalized radar phase and normalized sEMG, as well as the hysteresis curve in Fig. 10, we accept our second hypothesis. Specifically, this supports the claim that RMG is analogous to SMG.

The final observation common across our study and the studies in [12] and [39] was that the rate of muscle deformation was typically higher during the ON stage compared with the OFF stage. As in [12] however, this effect was not always observed. It was almost exclusively observed in participant one. In [12], this data artifact was attributed to the low frame rate (8 Hz) of the ultrasound imaging system and the inability of the participants to reduce torque smoothly. In our study, the muscle deformation was sampled at the slow time frequency of 200 Hz, which is more than 20 times that in [12] and thus the sampling frequency cannot be a limiting factor in our system. Instead, this limitation is probably due to participants 2 and 3 not relaxing the vastus lateralis smoothly.

VI. Conclusions and Limitations

Based on the foregoing results and discussions, we argue the radar phase signal we recover is the muscle deformation signal recovered through SMG. The proposed system can be used to relay information about human motions to computers, i.e., for human-computer-interaction, e.g., in AR/VR applications. In addition to routine isometric contractions during neurological and orthopaedic rehabilitation, AR/VR applications are another avenue in which our system is immediately useful.

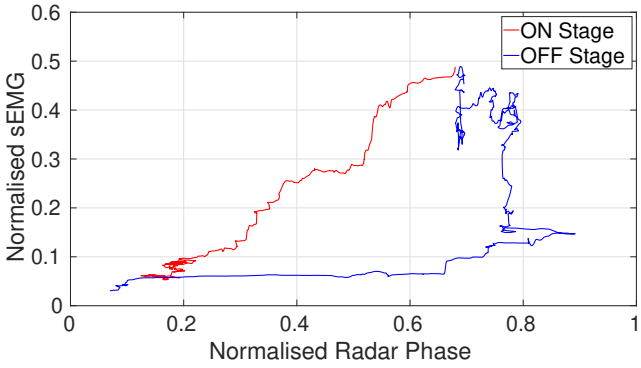

Fig. 10: Presented here is the normalised sEMG data from the illustrative trial and illustrative contraction-relaxation cycle plotted against the corresponding normalised radar phase from participant one. Only the ON and OFF stages of the contraction-relaxation cycle are presented. The part of the cycle when the contraction is held is not depicted. The hysteresis curve observed here is characteristic and well known in biomechanics [12] [39].

Our system is limited to monitoring muscle activity only for isometric contractions. Another limitation of our approach was that the recovered muscle deformation was prone to drift. Meaning that after contraction, the radar phase did not return back to 0 rad even though the muscle was relaxed (see Fig. 6). This happens because after every contraction, the muscle does not return to exactly the same position relative to the radar-camera rig as it was before the contraction. Though an effort was made by each participant to avoid translation of the leg, the leg was not strapped in place. The SMG approach is also prone to this drift problem as demonstrated in [4], [13] and [19]. A limitation of not only our implementation but the approach in general is that it cannot be used to monitor the muscle activity of deep muscles.

In future, the proposed technique will inform the analysis (e.g., of the gait) of humans during contact sporting activities such as rugby, where contact approaches are impractical, and thus provide athletes with information to improve their performance, prevent and facilitate rehabilitation from injuries. Similarly, our system will inform gait analysis of animals in the wild, inform biomechanics research, diagnosis and rehabilitation efforts.

For future work, we plan on extending our approach to enable RBM cancellation and thus enable the monitoring of muscles during eccentric and concentric contractions, as well

as the tracking and monitoring of muscle activity for mobile participants. Specifically, if the varying range of the target is known, say from a calibrated stereo-camera pair (see Fig. 5), then the radar phase signal can be computed with the beat frequency, f_b, updated using the range information.

APPENDIX

Range (Discrete) Fast Fourier Transform (Range FFT) for Range Bin Selection

Mathematically, the Range (Discrete) Fast Fourier Transform (Range FFT) is

$$X_k = \sum_{n=0}^{N-1} x_n e^{-j2\pi \frac{k}{N} n}, \tag{17}$$

where k is the frequency index, $x_n = S_B(iT + n \cdot T_s), n \in \{0, 1, 2, ..., N-1\}$ is the discretised received chirp, N is the number of samples per received chirp and $T_s = \frac{1}{f_s}$ is the period at which the received chirp has been sampled.

Dividing and multiplying by T_s in (17) gives

$$X_k = \sum_{n=0}^{N-1} x_n e^{-j2\pi \frac{k}{NT_s} nT_s}. \tag{18}$$

If we let $\frac{k}{NT_s} = \frac{k}{N} f_s = f_k$ and substitute into (18) the correct expression for x_n, we get

$$\begin{aligned} X_{f_k} &= \sum_{n=0}^{N-1} A_R e^{j2\pi f_b nT_s} e^{-j2\pi f_k nT_s} e^{j\varphi_i} \\ &= A_R e^{j\varphi_i} \sum_{n=0}^{N-1} e^{j2\pi (f_b - f_k) nT_s}. \end{aligned} \tag{19}$$

If $f_k = f_b$, then

$$X_{f_k} = N A_R e^{j\varphi_i} \tag{20}$$

because $\sum_{n=0}^{N-1} e^{j2\pi(f_b - f_k)nT_s} = N$. Therefore, at the beat frequency, the Range FFT coefficient has magnitude $|X_{f_k}| = NA_R$.

However, if $f_k \neq f_b$, then we can let $z = e^{j2\pi(f_b - f_k)T_s}, z \in \mathbf{C}$. Then by noticing that our sum is a geometric sum, we have

$$\sum_{n=0}^{N-1} e^{j2\pi(f_b - f_k)nT_s} = \sum_{n=0}^{N-1} z^n = 1 + z + z^2 + z^3 + ... + z^{N-1}. \tag{21}$$

Letting $|\sum_{n=0}^{N-1} e^{j2\pi(f_b - f_k)nT_s}| = N^*$ and applying the triangle inequality on (21) gives

$$\left| \sum_{n=0}^{N-1} e^{j2\pi(f_b - f_k)nT_s} \right| \leq |1| + |z| + |z^2| + ... + |z^{N-1}| = N. \tag{22}$$

REFERENCES

[1] R. H. Chowdhury, M. B. I. Reaz, M. A. B. M. Ali, A. A. A. Bakar, K. Chellappan, and T. G. Chang, "Surface electromyography signal processing and classification techniques," *Sensors (Basel)*, vol. 13, no. 9, pp. 12 431–12 466, Sep. 2013.

[2] R. B. Woodward, M. J. Stokes, S. J. Shefelbine, and R. Vaidyanathan, "Segmenting mechanomyography measures of muscle activity phases using inertial data," *Sci. Rep.*, vol. 9, no. 1, p. 5569, Apr. 2019.

[3] L. A. Hallock, A. Kato, and R. Bajcsy, "Empirical quantification and modeling of muscle deformation: Toward ultrasound-driven assistive device control," in *2018 IEEE International Conference on Robotics and Automation (ICRA)*, 2018, pp. 1825–1832.

[4] L. A. Hallock, B. Sud, C. Mitchell, E. Hu, F. Ahamed, A. Velu, A. Schwartz, and R. Bajcsy, "Toward real-time muscle force inference and device control via optical-flow-tracked muscle deformation," *IEEE Trans. Neural Syst. Rehabil. Eng.*, vol. 29, pp. 2625–2634, Dec. 2021.

[5] K. Li, M. Tucker, R. Gehlhar, Y. Yue, and A. D. Ames, "Natural multicontact walking for robotic assistive devices via musculoskeletal models and hybrid zero dynamics," *IEEE Robotics and Automation Letters*, vol. 7, no. 2, pp. 4283–4290, 2022.

[6] Y. Masuda and M. Ishikawa, "Autonomous intermuscular coordination and leg trajectorygeneration of neurophysiology-based quasi-quadruped robot," in *2020 IEEE/SICE International Symposium on System Integration (SII)*, 2020, pp. 1123–1128.

[7] R. Merletti and D. Farina, Eds., *Surface Electromyography*, ser. IEEE Press Series on Biomedical Engineering. Nashville, TN: John Wiley & Sons, Apr. 2016.

[8] C. Orizio, "Muscle sound: bases for the introduction of a mechanomyographic signal in muscle studies," *Crit. Rev. Biomed. Eng.*, vol. 21, no. 3, pp. 201–243, 1993.

[9] D. T. Barry, S. R. Geiringer, and R. D. Ball, "Acoustic myography: A noninvasive monitor of motor unit fatigue," *Muscle & Nerve*, vol. 8, no. 3, pp. 189–194, Mar. 1985. [Online]. Available: https://doi.org/10.1002/mus.880080303

[10] S. Casaccia, L. Scalise, L. Casacanditella, E. P. Tomasini, and J. W. Rohrbaugh, "Non-contact assessment of muscle contraction: Laser Doppler Myography," in *2015 IEEE International Symposium on Medical Measurements and Applications, MeMeA 2015, Torino, Italy, May 7-9, 2015*. IEEE, 2015, pp. 610–615. [Online]. Available: https://doi.org/10.1109/MeMeA.2015.7145276

[11] J. W. Rohrbaugh, E. J. Sirevaag, and E. J. Richter, "Laser Doppler vibrometry measurement of the mechanical myogram," *Rev. Sci. Instrum.*, vol. 84, no. 12, p. 121706, Dec. 2013.

[12] J. Shi, Y.-P. Zheng, Q.-H. Huang, and X. Chen, "Continuous monitoring of sonomyography, electromyography and torque generated by normal upper arm muscles during isometric contraction: sonomyography assessment for arm muscles," *IEEE Trans. Biomed. Eng.*, vol. 55, no. 3, pp. 1191–1198, Mar. 2008.

[13] A. T. Kamatham, M. Alzamani, A. Dockum, S. Sikdar, and B. Mukherjee, "A simple, drift compensated method for estimation of isometric force using sonomyography," in *Sensing Technology*, ser. Lecture notes in electrical engineering. Cham: Springer International Publishing, 2022, pp. 355–366.

[14] L. Brausch, H. Hewener, and P. Lukowicz, "Classifying muscle states with one-dimensional radio-frequency signals from single element ultrasound transducers," *Sensors*, vol. 22, no. 7, 2022. [Online]. Available: https://www.mdpi.com/1424-8220/22/7/2789

[15] A. Manca, A. Cereatti, L. Bar-On, A. Botter, U. Della Croce, M. Knaflitz, N. A. Maffiuletti, D. Mazzoli, A. Merlo, S. Roatta, A. Turolla, and F. Deriu, "A survey on the use and barriers of surface electromyography in neurorehabilitation," *Front. Neurol.*, vol. 11, p. 573616, Oct. 2020.

[16] C. Orizio, M. Gobbo, A. Veicsteinas, R. Baratta, B. Zhou, and M. Solomonow, "Transients of the force and surface mechanomyogram during cat gastrocnemius tetanic stimulation," *European Journal of Applied Physiology*, vol. 88, no. 6, pp. 601–606, Feb. 2003.

[17] P. Regtien and E. Dertien, "9 - acoustic sensors," in *Sensors for Mechatronics (Second Edition)*, 2nd ed., P. Regtien and E. Dertien, Eds. Elsevier, 2018, pp. 267–303. [Online]. Available: https://www.sciencedirect.com/science/article/pii/B9780128138106000094

[18] H. Azhari, "Special imaging techniques," in *Basics of Biomedical Ultrasound for Engineers*. Hoboken, NJ, USA: John Wiley & Sons, Inc., Apr. 2010, p. 313.

[19] L. A. Hallock, A. Velu, A. Schwartz, and R. Bajcsy, "Muscle deformation correlates with output force during isometric contraction," in *2020 8th IEEE RAS/EMBS International Conference for Biomedical Robotics and Biomechatronics (BioRob)*, 2020, pp. 1188–1195.

[20] T. A. McMahon, *Muscles, reflexes, and locomotion*. Princeton, NJ: Princeton University Press, Apr. 1984.

[21] V. C. Chen, *The micro-Doppler effect in radar the micro-Doppler effect in radar*, 2nd ed. Norwood, MA: Artech House, Feb. 2019.

[22] P. Zhao, C. X. Lu, B. Wang, C. Chen, L. Xie, M. Wang, N. Trigoni, and A. Markham, "Heart rate sensing with a robot mounted mmWave radar," in *International Conference on Robotics and Automation (ICRA)*, 2020.

[23] F. Adib, H. Mao, Z. Kabelac, D. Katabi, and R. C. Miller, "Smart homes that monitor breathing and heart rate," in *Proceedings of the 33rd Annual ACM Conference on Human Factors in Computing Systems*. New York, NY, USA: ACM, Apr. 2015.

[24] Y. Xiong, Z. Peng, G. Xing, W. Zhang, and G. Meng, "Accurate and robust displacement measurement for FMCW radar vibration monitoring," *IEEE Sensors Journal*, vol. 18, no. 3, pp. 1131–1139, 2018.

[25] C. Gu, G. Wang, Y. Li, T. Inoue, and C. Li, "A hybrid radar-camera sensing system with phase compensation for random body movement cancellation in doppler vital sign detection," *IEEE Transactions on Microwave Theory and Techniques*, vol. 61, no. 12, pp. 4678–4688, 2013.

[26] B.-K. Park, S. Yamada, and V. Lubecke, "Measurement method for imbalance factors in direct-conversion quadrature radar systems," *IEEE Microwave and Wireless Components Letters*, vol. 17, no. 5, pp. 403–405, 2007.

[27] A. Singh, X. Gao, E. Yavari, M. Zakrzewski, X. H. Cao, V. M. Lubecke, and O. Boric-Lubecke, "Data-based quadrature imbalance compensation for a CW Doppler radar system," *IEEE Transactions on Microwave Theory and Techniques*, vol. 61, no. 4, pp. 1718–1724, 2013.

[28] Z. Xu, C. Shi, T. Zhang, S. Li, Y. Yuan, C.-T. M. Wu, Y. Chen, and A. Petropulu, "Simultaneous monitoring of multiple people's vital sign leveraging a single phased-MIMO radar," *IEEE Journal of Electromagnetics, RF and Microwaves in Medicine and Biology*, vol. 6, no. 3, pp. 311–320, 2022.

[29] M. Alizadeh, G. Shaker, J. C. M. de Almeida, P. P. Morita, and S. Safavi-Naeini, "Remote monitoring of human vital signs using mmWave FMCW radar," *IEEE Access*, vol. 7, pp. 54 958–54 968, 2019.

[30] G. Shafiq and K. C. Veluvolu, "Surface chest motion decomposition for cardiovascular monitoring," *Scientific Reports*, vol. 4, no. 1, May 2014. [Online]. Available: http://dx.doi.org/10.1038/srep05093

[31] S. Rao, "MIMO radar (rev. a) - Texas Instruments," Jul 2018. [Online]. Available: https://www.ti.com/lit/an/swra554a/swra554a.pdf

[32] "IWR6843ISK Evaluation board — TI.com — ti.com," https://www.ti.com/tool/IWR6843ISK, [Accessed 14-Jun-2023].

[33] "DCA1000EVM Evaluation board — TI.com — ti.com," https://www.ti.com/tool/DCA1000EVM, [Accessed 14-Jun-2023].

[34] "MMWAVEICBOOST Evaluation board — TI.com — ti.com," https://www.ti.com/tool/MMWAVEICBOOST, [Accessed 14-Jun-2023].

[35] P. W. Hodges, L. H. M. Pengel, R. D. Herbert, and S. C. Gandevia, "Measurement of muscle contraction with ultrasound imaging," *Muscle Nerve*, vol. 27, no. 6, pp. 682–692, Jun. 2003.

[36] "Least-Squares (Model Fitting) Algorithms - MATLAB &; Simulink - MathWorks United Kingdom — uk.mathworks.com," https://uk.mathworks.com/help/optim/ug/least-squares-model-fitting-algorithms.html, [Accessed 14-Jun-2023].

[37] A. I. Kostyukov, "Muscle dynamics: dependence of muscle length on changes in external load," *Biol. Cybern.*, vol. 56, no. 5-6, pp. 375–387, 1987.

[38] M. Dornowski, O. V. Lehedza, V. S. Mishchenko, and A. V. Gorkovenko, "Hysteresis in EMG activity of muscles of the human upper limb at rotations of the isometric effort vector," *Neurophysiology*, vol. 49, no. 4, pp. 308–312, Aug. 2017.

[39] C. Orizio, M. Gobbo, A. Veicsteinas, R. V. Baratta, B. H. Zhou, and M. Solomonow, "Transients of the force and surface mechanomyogram during cat gastrocnemius tetanic stimulation," *Eur. J. Appl. Physiol.*, vol. 88, no. 6, pp. 601–606, Feb. 2003.

[40] V. I. Sobolev, V. V. Trush, K. A. Litvyak, and I. N. Morozova, "Hysteresis properties of EMG activity of the shoulder belt and shoulder muscles at the development of isometric efforts by the human arm," *Neurophysiology*, vol. 47, no. 1, pp. 61–70, Feb. 2015.

Kukhokuhle Tsengwa received the B.Sc. degree in mechatronics engineering from the University of Cape Town (UCT) in 2020. He is set to graduate from the M.Sc. degree in electrical engineering from UCT in 2023. He is currently pursuing the PhD degree at the Oxford Robotics Institute at the University of Oxford working on control barrier functions for obstacle avoidance for walking robots and supported by the Rhodes Trust. His research interests include control, dynamical systems and signal processing.

Stephen Paine holds an M.Sc. (Eng) in radar and electronic defense specializing in RF and antenna design, and a Ph.D. (Eng) specializing in passive radar and electronic warfare from the University of Cape Town. He is currently a Lecturer with the Department of Electrical Engineering at the University of Cape Town, where he is also the Head of the Radar and Remote Sensing Group (RRSG). He has previously worked in industry in South Africa and Switzerland, with research interests in the field of radar, remote sensor fusion, signal processing, and automotive systems. He is a Junior Member of the IEEE.

Fred Nicolls is an Associate Professor in the Department of Electrical Engineering at the University of Cape Town, Cape Town, South Africa. His research interests include signal and image processing, optical sensing, and computer vision, often with a particular focus on medical imaging and medical technologies.

Yumna Albertus received a Ph.D Exercise Science in 2008 from the University of Cape Town. She is currently an Associate Professor with the Department of Human Biology, University of Cape Town. She is a research member of the Health, Physical Activity, Lifestyle and Sport Research Centre (HPALS) and UCT Neuroscience Institute. Her research interests include neuromuscular physiology (involving both bipolar and high density sEMG) in performance and clinical conditions, specifically spinal cord injury and Cerebral Palsy. She was awarded UCT's Research Leadership Award, one of 10 female researchers recognised for their impactful research. She is the current Chair of the South African Society of Biomechanics and the African representative on the International Society of Biomechanics Executive Board.

Amir Patel (Senior Member, IEEE) received a B.Sc. degree in mechatronics, an M.S. degree in control engineering, and a Ph.D. degree in mechatronics from the University of Cape Town, Cape Town, South Africa, in 2009, 2011, and 2014, respectively. He is currently an Associate Professor with the Department of Computer Science, University College London. He has held Visiting Researcher positions at Carnegie Mellon University (2018) USA, Johns Hopkins University (2018), and University of Oxford (2023). His research interests include maneuverability in legged animals, bioinspired robotics, optimal control, and novel sensing systems. Dr. Patel was awarded the Claude Leon Merit Award (2016), the Oppenheimer Memorial Trust Fellowship (2018 and 2022) and one of the first two Africans to receive the Google Research Scholar award (2019).